A dynamic micromixer for arbitrary control of disguised chemical selectivity†

Karla K. Cotí,‡[ab] Yanju Wang,‡[ac] Wei-Yu Lin,[a] Chia-Chun Chen,[a] Zeta Tak For Yu,[a] Kan Liu,[a] Clifton K.-F. Shen,[a] Matthias Selke,*[c] Anchi Yeh,*[d] Weixing Lu*[a] and Hsian-Rong Tseng*[a]

Received (in Cambridge, UK) 17th March 2008, Accepted 21st April 2008
First published as an Advance Article on the web 23rd May 2008
DOI: 10.1039/b804530e

A new type of dynamic micromixer combining the concepts of parallel multi-lamination and hydrodynamic focusing was developed for arbitrary control of disguised chemical selectivity.

Microreactors are microscopic reaction settings that exhibit unique properties *versus* traditional macroscopic environments: advantages of microreactors include reduced reagent consumption, high surface-area-to-volume ratios and improved control over mass and heat transfer.[1–8] In addition, fluidic physical phenomena in the microreactors are dramatically different from those observed in the macroscopic reaction apparatuses.[9–11] For instance, the inertial effect in the microfluidic environment is negligible (due to a low value of Reynolds number, *Re*), and thus fluid transport is dictated by fluid viscosity, leading to laminar flow in microchannels. A microfluidics-based reactor is known to be a turbulence-free system, in which diffusion-driven mixing is relatively slow. As a result, one of the most challenging issues in the field of microreactor design is to facilitate mixing in stand-alone devices. Over the past decades enormous efforts have been devoted to develop micromixers (one type of microreactor) that can be categorized into either active or passive ones.[12] Unlike active micromixers, passive ones[13] do not require external power, are often composed of robust channel geometry or microstructures, and are developed upon straightforward concepts of increasing contact surfaces and/or shortening the distance for diffusion among different streams. For example, devices based on parallel[14–16] multi-lamination[12] have been developed to achieve efficient mixing.

Mixing may impact reaction outcomes.[17,18] A good example is the diazo coupling reaction[19] between 4-sulfono-benzenediazonium (**1**) and 1-naphthol (**2**) under alkaline conditions at room temperature. This reaction is known as a fast competitive consecutive reaction[20] (Scheme 1), where the selectivity between the two major reaction products (*i.e.*, monosubstituted product **3** and disubstituted product **4**) is not only determined by intrinsic reaction kinetics[21] ($k_1 = 1.2 \times 10^7$ M^{-1} s^{-1} and $k_2 = 2 \times 10^3$ M^{-1} s^{-1}) but also affected by the mixing rates. When reactants **1** and **2** are mixed in a macroscopic setting, the reaction solution is first fragmented by stir-induced turbulence. No matter what mixing approach (*e.g.*, hand mixing or mechanical stirring) is applied, in the best case scenario, the mean radii of the fragmentized solutions are approximately in the range of 100 to 1000 μm,[22,23] leading to a mixing time ranging from a millisecond to seconds. Consequently, the fast reaction between the **1** and **2** happens prior to complete homogeneous mixing to give a complicated reaction mixture containing reactant **2** and products **3** and **4**. This phenomenon is known as the disguised chemical selectivity.[20,24,25] In order to avoid the undesired disguised chemical selectivity, micromixers exhibiting fast mixing rates have been developed.[4,20]

In this paper, we introduce a new concept of a dynamic micromixer (Fig. 1), which combines the concepts of parallel[14–16,26] multi-lamination[12] and hydrodynamic focusing.[18,27] This dynamic mixer composed of 200 μm wide and 80 μm high microchannels was fabricated from poly-methylmethacrylate (PMMA) materials[28] or polydimethylsiloxane (PDMS)[8] (see ESI†). There are three geometrically defined sections in the device, including: (i) a hydrodynamic focusing region where reactant and isolation streams are introduced into the device through the nine inletting microchannels, (ii) a linear microchannel for controlled mixing, and (iii) a triple-branched junction for collecting the resulting reaction mixtures and bypassing the sheath streams. Fluorescence microscopy can be used to observe the flow behavior, and our microreactor, for the first time, can be utilized to control the disguised chemical selectivity a chemical reaction sequence, namely of the diazo coupling reaction between **1** and **2**.

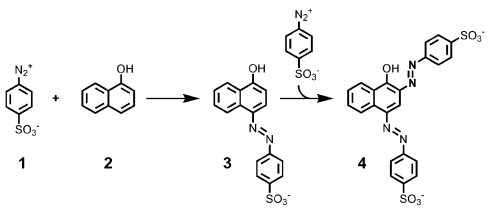

Scheme 1 A diazo-coupling reaction between 4-sulfono-1-phenyldiazonium tetrafluorobrate (**1**) and 1-naphthol (**2**).

[a] *Crump Institute for Molecular Imaging, Department of Molecular and Medical Pharmacology, David Geffen School of Medicine at UCLA, 700 Westwood Plaza, Los Angeles, CA 90095, USA. E-mail: hrtseng@mednet.ucla.edu. E-mail: wlu@mednet.ucla.edu*
[b] *Department of Chemistry and Biochemistry, University of California Los Angeles, 405 Hilgard Ave., Los Angeles, CA 90095, USA*
[c] *Department of Chemistry and Biochemistry, California State University, Los Angeles, 5151 University Drive, Los Angeles, CA 90032, USA. E-mail: mselke@calstatela.edu*
[d] *Department of Chemical and Material Engineering, Chengshiu University Niaosong, Kaohsiung County, 833, Taiwan. E-mail: acyeh@csu.edu.tw*

† Electronic supplementary information (ESI) available: Experimental. See DOI: 10.1039/b804530e

‡ These authors contributed equally to this work.

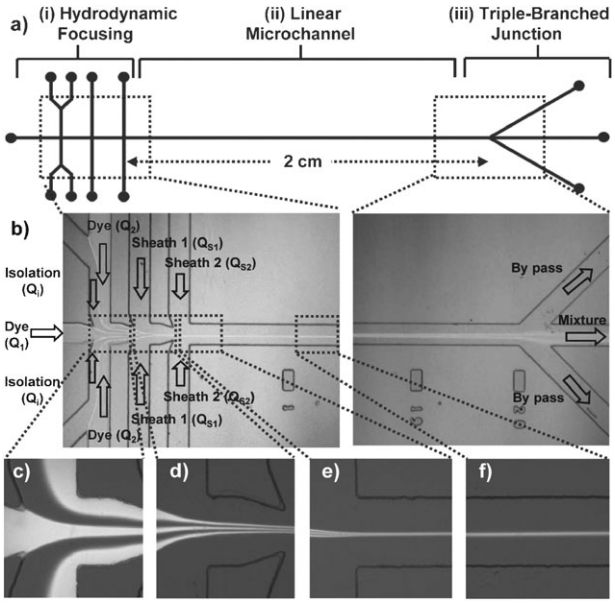

Fig. 1 (a) Schematic drawing of our dynamic microreactor composed of three geometrically defined sections: (a) (i) a hydrodynamic focusing region, (ii) a linear microchannel and (iii) a triple-branched junction. (b–f) Fluorescence images of the hydrodynamic focusing region and triple-branched junction.

To help visualize and characterize the mixing behavior (Fig. 1b–f) within the dynamic microreactor, an aqueous solution containing 5-carboxyfluorescein, was introduced into the reactor from the three reactant inlets along with an isolation solution (*i.e.*, Tris-HCl buffer), and two pairs of sheath streams (pure water) were utilized to compress the three fluorescent and two isolation streams to form a hydrodynamic focused beam (beam width = 9.8 μm) for diffusion-driven mixing. We define the stream compression ratio as α [$\alpha = (2Q_{S1} + 2Q_{S2})/(Q_1 + 2Q_i + 2Q_2)$, in this case $\alpha = 20$]. Fluorescence microscopy was employed to characterize the flow behavior. As shown in Fig. 1b, three fluorescent streams (representing reagent streams) and two isolation streams formed isolated and parallel laminar flows at the beginning section of the hydrodynamic focusing region.[29,30] Sequentially, these laminar flows were compressed into a much smaller characteristic length by two-step hydrodynamic focusing with sheath streams (Fig. 1d and e).[31] As a result, the diffusion distances among reactant streams decreased dramatically (Fig. 1f; in principle, each laminar flow can be compressed to as low as 50 nm[27]). Thus, diffusion-driven mixing results in a homogeneous reaction beam in the linear microchannel. It is important to note that the parabolic effect[32] associated with the interactions between reactant streams and microchannel walls has been significantly reduced due to the use of sheath flows which reduce contact areas between reactant streams and microchannel walls.

A systematic study on the relationship between α and the cross-sectional widths of the hydrodynamic focused beam (composed of the three fluorescent reactant and two isolation streams) was conducted (see ESI Fig. S1†). Our analyses show that at high α values fast mixing is achieved as suggested by the absence of a visible boundary in between the three fluorescent streams (inset micrographs shown in Fig. S1b†). In contrast, three distinct fluorescent streams were observed at low α values, indicating that more time is required to achieve complete mixing for larger diffusion distances. Here, we demonstrate that the mixing timing, mixing speed and entrance length of reagent solutions are determined by the distance between the three reactant streams as a function of the α values. Thus, the sheath streams play a role akin to dynamic channel walls, allowing arbitrary alternation of a virtual microchannel accommodating the five reactant/isolation streams with great precision and stability. These observations constitute the operational principles of our dynamic micromixer, which exhibits unique characteristics, including (i) adjustable mixing time covering from μs to ms, (ii) variable diffusion length, and tunable entrance length for each reactant, (iii) dramatically reduced parabolic effects[32] in microchannels, and (iv) dynamically confined reaction spaces at micro/nano scale. It is important to note the use of two-step hydrodynamic focusing confers flow stability to the micromixer compared to the one-step approaches.[33] We demonstrated a dynamic operation range covering the stream compression ratio from 1 to 55, corresponding to focused beam widths ranging from 88 to 4 μm. This dynamic mixing property of the microreactor was then utilized to perform fast competitive and consecutive reaction between **1** and **2** under controllable mixing rates. We are able to demonstrate tunable product distributions by methodically altering the mixing rates using the same device configuration.

To allow direct ^{1}H-NMR spectroscopic analyses of the products **3** and **4** obtained from the dynamic micromixer, the reactant/isolation/sheath solutions were prepared in a deuterated solvent mixture (D_2O/DMSO-d_6 = 8/2, v/v) buffered with Na_2CO_3 (10 mM) and $NaHCO_3$ (10 mM) to control the reaction condition at a pH value of 10. In our study (Fig. 2a) reactant **1** (30 mM) and **2**, (16 mM) were introduced into the respective inlets along with the two isolation streams at an identical flow rate of 1.0 μL min^{-1}, followed by hydrodynamic focusing using two pairs of sheath streams at variable flow rates ranging from 1.5 to 69 μL min^{-1}. By systematically increasing the sheath flows, we studied how different α values (from 1.0 to 55) affect the products distribution of the diazo coupling reaction. The resulting product mixtures were collected from the mixture outlet channel (see ESI Fig. S2b†) using NMR tubes, which were kept at −78 °C in the dark prior to ^{1}H-NMR spectroscopic analyses. As references, ^{1}H-NMR spectra of compounds **1**, **2**, **3** and **4** were recorded in the same buffered deuterated solvent mixture (Fig. S2b†). To determine the product distribution ratios (*i.e.*, $P_3/(2P_4 + P_3)$ and $P_4/(2P_4 + P_3)$, where P_3 and P_4 stand for the molar ratios for the products **3** and **4**, respectively) at different α values, we followed the chemical shifts centered at δ = 6.77 and 8.35 ppm, corresponding to the H_j proton of the products **3** and the H_x proton of the product **4**, respectively (see ESI, Fig. S2b†). The integrations of the ^{1}H-NMR signals gave the product molar ratios, P_3 and P_4, from which we calculated the product distribution ratios. It is important to note that where conventional methods fail at producing the product of interest, **3**, in high yields, our microreactor can produce **3** as the primary product. Fig. 2b and c summarize these

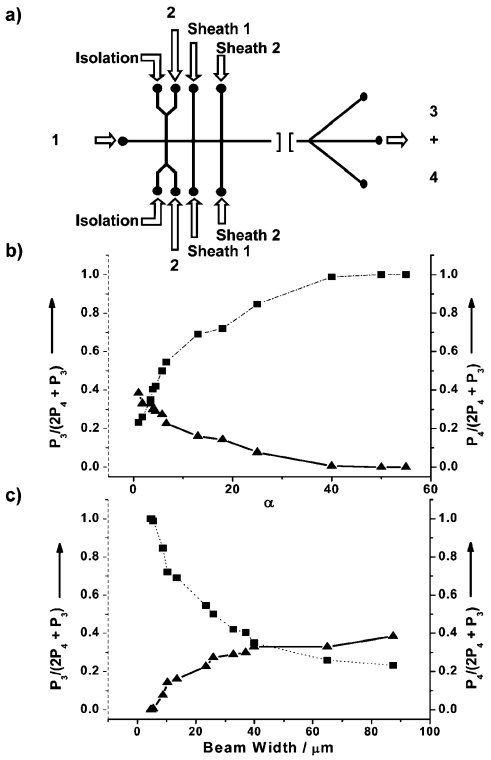

Fig. 2 (a) Competitive-consecutive diazo-coupling reaction between **1** and **2** were carried out in the dynamic reactor at different stream compression ratios (α). (b) Distribution plots of **3** ($P_3/(2P_4 + P_3)$, squares, dashed line) and **4** ($P_4/(2P_4 + P_3)$, triangles, solid line) as a function of (c) α values and (d) focused beam widths.

experimental results, illustrating the relationship between the stream compression ratio (α) and the resulting product distribution ratios. According to the results obtained in mixing behavior studies (Fig. S2b†) and keeping in mind that the α values and hydrodynamic focused beam widths are reciprocally related, the α values can be converted to the respective focused beam widths. Thus Fig. 2c, where the product distribution ratios are plotted against focused beam widths, better interprets the concept of our dynamic micromixer—*i.e.*, multi-lamination beams with variable widths for controllable mixing, allowing arbitrary control of the product distribution of a fast competitive consecutive reaction.[4,20]

In conclusion, the usefulness of the dynamic microreactor was confirmed by achieving control over the disguised chemical selectivity of the diazo reaction. It is conceivable that this dynamic micromixer can also provide a powerful platform to study particle and quantum dot formation, chemical and biological reaction kinetics and conduct biological analyses, all of which require precise control in reaction kinetics.

This research was supported by the DOD-Defense Threat Reduction Agency (W911NF0610243), the NIH-NCI Nano-Systems Biology Cancer Center (U54A119347). M.S. gratefully acknowledges support by the NSF-PREM Program (Award No. 0351848).

Notes and references

1. For reviews see (*a*) P. Watts and C. Wiles, *Chem. Commun.*, 2007, 443–467; (*b*) K. Geyer, J. D. C. Codee and P. H. Seeberger, *Chem.–Eur. J.*, 2006, **12**, 8434–8442; (*c*) J. Kobayashi, Y. Mori and S. Kobayashi, *Chem.–Asian J.*, 2006, **1**, 22–35; (*d*) M. Brivio, W. Verboom and D. N. Reinhoudt, *Lab Chip*, 2006, **6**, 329–344l; (*e*) P. Watts and C. Wiles, *Org. Biomol. Chem.*, 2007, **5**, 727–732.
2. K. Jensen, *Nature*, 1998, **393**, 735–737.
3. W. Ehrfeld, V. Hessel and H. Lowe, *Microreactors—New Technology for Modern Chemistry*, Wiley-VCH, New York, 2000.
4. G. M. Whitesides, *Nature*, 2006, **442**, 368–373.
5. J. Yoshida, A. Nagaki, T. Iwasaki and S. Suga, *Chem. Eng. Technol.*, 2005, **28**, 259–266.
6. A. K. Goetz, B. Scheffler, H. X. Chen, S. S. Wang, O. Suslov, H. Xiang, O. Brustle, S. N. Roper and D. A. Steindler, *Proc. Natl. Acad. Sci. U. S. A.*, 2006, **103**, 11063–11068.
7. A. J. deMello, *Nature*, 2006, **442**, 394–402.
8. (*a*) C. C. Lee, A. Elizarov, C. Y. J. Shu, Y. S. Shin, A. N. Dooley, J. Huang, A. Daridon, D. S. P. Wyatt, H. C. Kolb, O. N. Witte, N. Satyamurthy, J. R. Heath, M. E. Phelps, S. R. Quake and H. R. Tseng, *Science*, 2005, **310**, 1793–1796; (*b*) G. D. Sui and H. R. Tseng, *Nano Today*, 2006, 6–7; (*c*) J. Y. Wang, G. D. Sui, V. P. Mocharla, R. J. Lin, M. E. Phelps, H. C. Kolb and H. R. Tseng, *Angew. Chem., Int. Ed.*, 2007, **45**, 5276–5281; (*d*) S. Hou, S. Wang, Z. T. F. Yu, N. Q. M. Zhu, J. Sun, W.-Y. Lin, C. K.-F. Shen, X. Fang and H.-R. Tseng, *Angew. Chem., Int. Ed.*, 2008, **47**, 1072–1075.
9. E. M. Purcell, *Am. J. Phys.*, 1977, **45**, 3–11.
10. J. P. Brody, P. Yager, R. E. Goldstein and R. H. Austin, *Biophys. J.*, 1996, **71**, 3430–3441.
11. T. M. Squires and S. R. Quake, *Rev. Mod. Phys.*, 2005, **77**, 977–1026.
12. N. T. Nguyen and Z. G. Wu, *J. Micromech. Microeng.*, 2005, **15**, R1.
13. V. Hessel, H. Lowe and F. Schonfeld, *Chem. Eng. Sci.*, 2005, **60**, 2479–2501.
14. F. G. Bessoth, A. J. deMello and A. Manz, *Anal. Commun.*, 1999, **36**, 213–215.
15. Y. Xu, F. G. Bessoth, J. C. T. Eijkel and A. Manz, *Analyst*, 2000, **125**, 677–683.
16. M. C. Mitchell, V. Spikmans and A. J. de Mello, *Analyst*, 2001, **126**, 24–27.
17. K. Jahnisch, V. Hessel, H. Lowe and M. Baerns, *Angew. Chem., Int. Ed.*, 2004, **43**, 406–446.
18. Z. G. Wu and N. T. Nguyen, *Biomed. Microdevices*, 2005, **7**, 13–20.
19. (*a*) H. Hisamoto, T. Saito, M. Tokeshi, A. Hibara and T. Kitamori, *Chem. Commun.*, 2001, 2662–2663; (*b*) J. R. Bourne, C. Hilber and G. Tovstiga, *Chem. Eng. Commun.*, 1985, **37**, 293–314.
20. A. Nagaki, M. Togai, S. Suga, N. Aoki, K. Mae and J. Yoshida, *J. Am. Chem. Soc.*, 2005, **127**, 11666–11675.
21. J. R. Bourne, O. M. Kut and J. Lenzner, *Ind. Eng. Chem. Res.*, 1992, **31**, 949–958.
22. R. J. Ott and P. Rys, *Helv. Chim. Acta*, 1975, **58**, 2074–2093.
23. H. Okamoto, *Kagakusochi*, 2004, **9**, 74.
24. P. Rys, *Acc. Chem. Res.*, 1976, **9**, 345–351.
25. P. Rys, *Angew. Chem., Int. Ed. Engl.*, 1977, **16**, 807–884.
26. M. C. Mitchell, V. Spikmans, A. Manz and A. J. de Mello, *J. Chem. Soc., Perkin Trans. 1*, 2001, 514–518.
27. J. B. Knight, A. Vishwanath, J. P. Brody and R. H. Austin, *Phys. Rev. Lett.*, 1998, **80**, 3863–3866.
28. X. L. Zhu, G. Liu, Y. H. Guo and Y. C. Tian, *Microsyst. Technol.*, 2007, **13**, 403–407.
29. The isolation stream is important to prevent premixing of the reagents prior to hydrodynamic focusing thus having control of the reagents' mixing time.
30. H. Y. Park, X. Qiu, E. Rhoades, J. Korlach, L. W. Kwok, W. R. Zipfel, W. W. Webb and L. Pollack, *Anal. Chem.*, 2006, **78**, 4465–4473.
31. The shape of the reagent/isolation streams in Fig. 1d not only depends on the compression of the sheath streams but also that the shape of the channel reduces at the entrance of each inlet junction.
32. R. F. Ismagilov, A. D. Stroock, P. J. A. Kenis, G. Whitesides and H. A. Stone, *Appl. Phys. Lett.*, 2000, **76**, 2376–2378.
33. When one-step sheath flow compression was applied to generate a focused stream with a width smaller than 4 μm, the insatiability manifested in the form of shaky or discontinuous focused streams.

